

Pecore LM and Carrol TL (1990) Synchronization of chaotic systems. *Physical Review Letters* 64: 821–824.
 Roy R, *et al.* (1992) Dynamical control of a chaotic laser: experimental stabilization of a globally coupled system. *Physical Review Letters* 68: 1259–1262.

VanWiggeren GD and Roy R (1998) Communication with chaotic lasers. *Science* 279: 1198–1200.
 VanWiggeren GD and Roy R (1998) Optical communication with chaotic waveforms. *Physical Review Letters* 279: 1198–1200.

CHEMICAL APPLICATIONS OF LASERS

Contents

Detection of Single Molecules in Liquids
Diffuse-Reflectance Laser Flash Photolysis
Laser Manipulation in Polymer Science
Nonlinear Spectroscopies
Photodynamic Therapy of Cancer
Pump and Probe Studies of Femtosecond Kinetics
Time-Correlated Single-Photon Counting
Transient Holographic Grating Techniques in Chemical Dynamics

Detection of Single Molecules in Liquids

A J de Mello, J B Edel and E K Hill, Imperial College of Science, Technology and Medicine, London, UK

© 2005, Elsevier Ltd. All Rights Reserved.

Introduction

A significant challenge facing experimentalists in the physical and biological sciences is the detection and identification of single molecules. The ability to perform such sensitive and selective measurements is extremely valuable in applications such as DNA analysis, immunoassays, environmental monitoring, and forensics, where small sample volumes and low analyte concentrations are the norm. More generally, most experimental observations of physical systems provide a measurement of ensemble averages, and yield information only on mean properties. In contrast, single molecule measurements permit observation of the interactions and behavior of a heterogeneous population in real time.

Over the past few years a number of techniques with sufficient sensitivity have been developed to detect single molecules. Scanning probe microscopies

(most notably scanning tunneling microscopy and atomic force microscopy) have been used to great effect in the analysis of surface bound species, but for the detection of single molecules in liquids, optical methods incorporating the measurement of absorption or emission processes, have proved most successful.

The Absorption–Emission Cycle

The key concept underlying most emissive approaches to single molecule detection is that a single molecule can be cycled repeatedly between its ground state and an excited electronic state to yield multiple photons. The process can be understood by reference to [Figure 1](#). Fluorescence emission in the condensed phase can be described using a four-step cycle. Excitation from a ground electronic state to an excited state is followed by rapid (internal) vibrational relaxation. Subsequently, radiative decay to the ground state is observed as fluorescence emission and is governed by the excited state lifetime. The final stage is internal relaxation back to the original ground state. Under saturating illumination, the rate-limiting step for this cycle is governed by the fluorescence lifetime (τ_f), which is typically of the order of a few nanoseconds. If a single molecule diffuses through an illuminated zone (e.g., the focus of a laser beam) it may reside in that

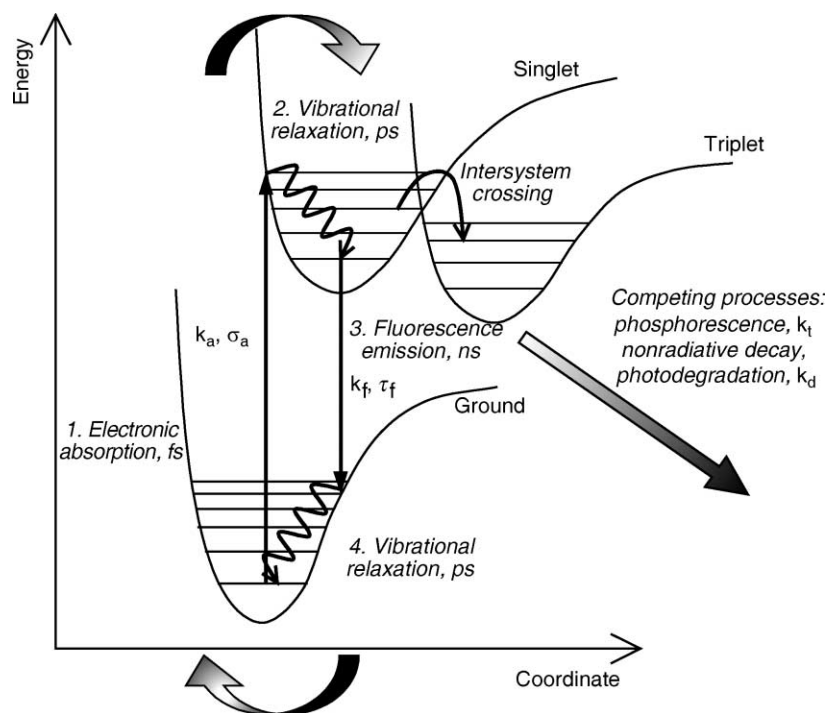


Figure 1 Schematic illustration of the molecular absorption–emission cycle and timescales for the component processes. Competing processes that may reduce the ultimate photon yield are also shown.

region for several milliseconds. The rapid photon absorption–emission cycle may therefore be repeated many times during the residence period, resulting in a burst of fluorescence photons as the molecule transits the beam. The burst size is limited theoretically by the ratio of the beam transit time (τ_r) and the fluorescence lifetime:

$$N_{\text{photons}} = \frac{\tau_r}{\tau_f} \quad [1]$$

For typical values of τ_r (5 ms) and τ_f (5 ns) up to one million photons may be emitted by the single molecule. In practice, photobleaching and photodegradation processes limit this yield to about 10^5 photons. Furthermore, advances in optical collection and detection technologies enable registration of about 1–5% of all photons emitted. This results in a fluorescence burst signature of up to a few thousand photons or photoelectrons.

Successful single molecule detection (SMD) depends critically on the optimization of the fluorescence burst size and the reduction of background interference from the bulk solvent and impurities. Specifically a molecule is well suited for SMD if it is efficiently excited by an optical source (i.e., possesses a large molecular absorption cross-section at the wavelength of interest), has a high fluorescence quantum efficiency (favoring radiative deactivation

of the excited state), has a short fluorescence lifetime, and is exceptionally photostable.

Ionic dyes are often well suited to SMD as fluorescence quantum efficiencies can be close to unity and fluorescence lifetimes below 10 nanoseconds. For example, xanthene dyes such as Rhodamine 6G and tetramethyl-rhodamine isothiocyanate are commonly used in SMD studies. However, other highly fluorescent dyes such as fluorescein are unsuitable for such applications due to unacceptably high photodegradation rate coefficients. Furthermore, some solvent systems may enhance nonradiative processes, such as intersystem crossing, and yield significant reduction in the photon output. Structures of three common dyes suitable for SMD are shown in Figure 2.

Signal vs Background

The primary challenge in SMD is to ensure sufficient reduction in background levels to enable discrimination between signal and noise. As an example, in a 1 nM aqueous dye solution each solute molecule occupies a volume of approximately 1 fL. However, this same volume also contains in excess of 10^{10} solvent molecules. Despite the relatively small scattering cross-section for an individual water molecule ($\sim 10^{-28} \text{ cm}^2$ at 488 nm), the cumulative scattering

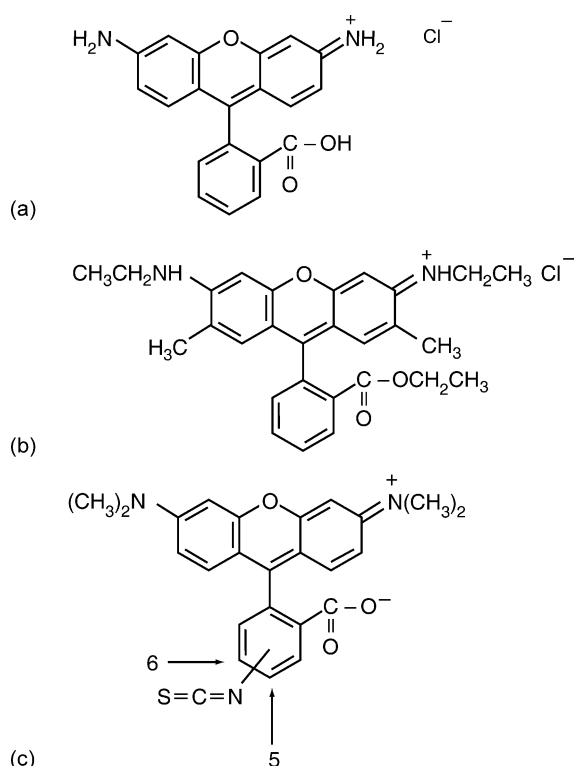


Figure 2 Structures of common dye molecules suitable for SMD in solution: (a) 3,6-diamino-9-(2-carboxyphenyl)-chloride (rhodamine 110); (b) 9-(2-(ethoxycarbonyl)phenyl)-3,6-bis(ethylamino)-2,7-dimethyl chloride (rhodamine 6G); (c) 9-(2-carboxyisothiocyanatophenyl)-3,6-bis(dimethylamino)-inner salt (tetramethylrhodamine-5-(and-6)-isothiocyanate).

signal from the solvent may swamp the desired fluorescence signal. The principal method of reducing the solvent background is to minimize the optical detection volume: the signal from a single molecule is independent of probe volume dimensions, but the background scales proportionally with the size of the detection region. Although there are several experimental approaches to SMD in solution, several factors hold common:

1. Tiny detection volumes (10^{-12} – 10^{-15} L) are used to reduce background signals.
2. A low analyte concentration combined with the small observation volume, ensures that less than one analyte molecule is present in the probe volume on average.
3. High-efficiency photon collection (optics) and detection maximize the proportion of the isotropic fluorescence burst that is registered.
4. Background reduction methods are employed to improve signal-to-noise ratios. These include: optical rejection of Raman and Rayleigh scatter, time-gated discrimination between prompt scatter and delayed emission, and photobleaching of the solvent immediately before detection.

The minute volumes within which single molecules are detected can be generated in a variety of ways. Picoliter volumes can be defined by mutually orthogonal excitation and detection optics focused in a flowing stream. Much smaller, femtoliter probe volumes are generated using confocal microscopes. At this level, background emission is significantly reduced and high signal-to-noise ratios can be achieved. Confocal detection techniques are versatile and have been widely adopted for SMD in freely diffusing systems. Consequently, confocal methods will be discussed in detail in this article. The other general approach to performing SMD in solution involves the physical restriction of single molecules within defined volumes. Of particular note are techniques where single molecules are confined within a stream of levitated microdroplets. Droplet volumes are typically less than 1 fL and imaging of the entire microdroplet enables single molecule fluorescence to be contrasted against droplet ‘blanks’ with good signal-to-noise. Furthermore, since molecules are confined within discrete volumes, the technique can be utilized for high-efficiency molecular counting applications. More recently, spatial confinement of molecules in capillaries and micro-fabricated channels (with submicron dimensions) has been used to create probe volumes between 1 fL and 1 pL, and immobilized molecules on surfaces have been individually probed using wide-field microscopy with epi-illumination or evanescent wave excitation.

Single Molecule Detection using Confocal Microscopy

As previously stated, the confocal fluorescence microscope is an adaptable and versatile tool for SMD. In its simplest form, a confocal microscope is one in which a point light source, a point focus in the object plane, and a pinhole detector are all confocal with each other. This optical superposition generates superior imaging properties and permits definition of ultra-small probe volumes. The concepts behind a basic confocal microscope and its use in SMD are schematically illustrated in Figure 3. Coherent light (typically from a laser and tuned to an optical transition of the molecule under investigation) behaves as a point light source and is focused into a sample chamber using a high-numerical aperture objective lens. As a single molecule traverses the laser beam it is continuously cycled between the ground and an excited electronic state, emitting a burst of fluorescence photons. Fluorescence emission is isotropic (spontaneous emission), so photons are emitted in all directions (4π steradians).

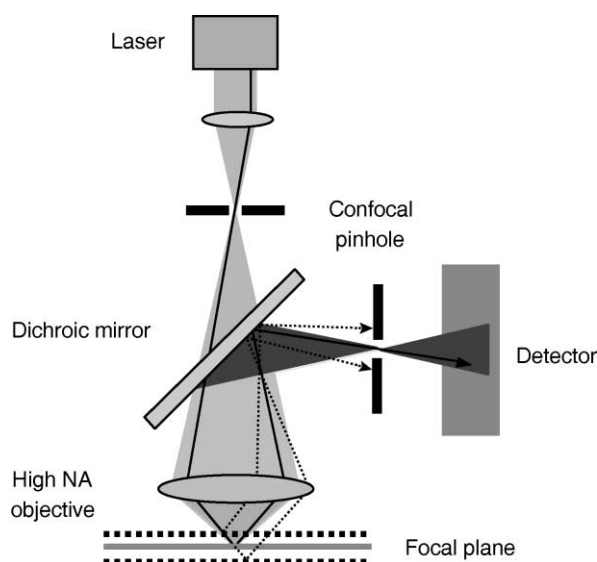


Figure 3 Principle of confocal detection. A confocal pinhole only selects light that emanates from the focal region. Dashed lines indicate paths of light sampled above and below the focal plane that are rejected by the pinhole. The solid ray derives from the focal point, and is transmitted through the pinhole to a detector.

Consequently, the high numerical aperture is used to collect as large a fraction of photons emitted from the focal plane as possible. Designing the objective to be used with an immersion medium, such as oil, glycerin, or water, can dramatically increase the objective numerical aperture, and thus the number of collected photons. Light collected by the objective is then transmitted towards a dichroic beam splitter. In the example shown, fluorescence photons (of lower energy) are reflected towards the confocal detector pinhole, whereas scattered radiation (of higher energy) is transmitted through the dichroic towards the light source. Creation of a precise optical probe volume is effected through the definition of the confocal pinhole. The detector is positioned such that only photons that pass through the pinhole are detected. Consequently, light emanating from the focal plane in the sample is transmitted through the pinhole and detected, whereas light not deriving from the focal plane is rejected by the aperture, and therefore not detected (Figure 3).

To ensure that the maximum number of photons are detected by the system, high efficiency detectors must be used. Photomultiplier tubes (the most common detectors for light-sensing applications) are robust and versatile but have poor detection efficiencies (approximately 5% of all photons that fall on the photocathode yield an electrical signal). Consequently, the most useful detectors for SMD (or low light level) applications are single photon-counting

avalanche photodiodes (SPADs). A SPAD is essentially a p–n junction reverse biased above the breakdown voltage, that sustains an avalanche current when triggered by a photon-generated carrier. Detection efficiencies for typical SPADs are normally between 60–70% and are thus ideal for SMD in solution. An approximation of the overall detection efficiency of a confocal system for SMD can be made using eqn [2], which incorporates an estimation of photon losses at all stages of the collection/detection process. Typical transmission efficiencies for each step are also shown.

overall detection efficiency	objective collection efficiency	dichroic transmission coefficient	additional optical losses	detector efficiency
0.06	0.24	0.9	0.5	0.6

[2]

Optical Probe Volumes

The precise nature of the probe volume is determined by the image of the pinhole in the sample and the spherical aberration of the microscope objective. Routinely, confocal probe volumes are approximated as resembling a cylinder with a radius defined by the diffraction-limited waist of a Gaussian beam. This approximation is useful when the incident beam is narrow or not tightly focused. However, when the radius of the incident beam is large, the corresponding diffraction limited focus is narrowed, and the probe volume more closely resembles a pair of truncated cones. Figure 4a illustrates the dependence of the curvature of the $1/e^2$ intensity contour on the collimated beam radius.

Consequently, it is clear that a simple cylindrical approximation for the probe volume breaks down for wide, tightly focused beams. If a broad incident beam (diameter > 1.5 mm) is used, a large noncylindrical contribution to the probe volume is anticipated and a more appropriate model is required. An alternative and more accurate model for the confocal probe volume considers the Gaussian profile of the focused beam. The $1/e^2$ intensity contour radius of a Gaussian waveform with wavelength λ , at some distance z from the beam waist radius w_0 , is given by eqn [3]:

$$w(z) = w_0 \sqrt{1 + \left(\frac{\lambda z}{\pi w_0^2} \right)^2} \quad [3]$$

In this case, the probe volume V is given by the volume of rotation of $w(z)$ around the z -axis between Z' and $-Z'$. The volume of rotation can therefore be

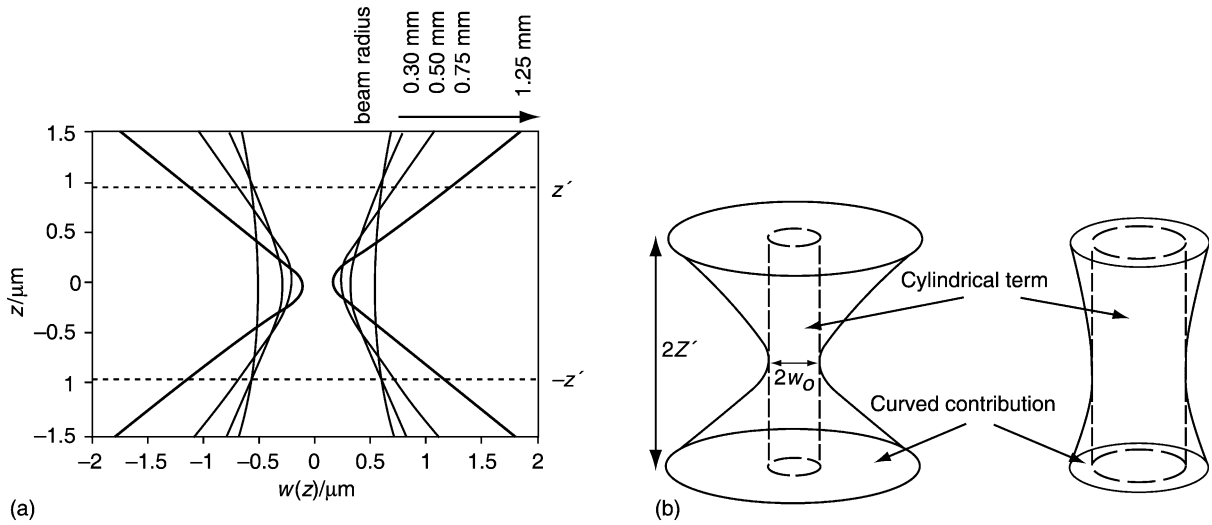


Figure 4 (a) $1/e^2$ Gaussian intensity contours plotted for a series of laser beam radii ($\lambda = 488$ nm, $f = 1.6$ mm, $n = 1.52$). (b) Cylindrical and curved components of the Gaussian probe volume. The curved contribution is more significant for larger beam radii and correspondingly tight beam waists.

simply defined according to,

$$V = \int_{-Z'}^{Z'} \pi w(z)^2 dz \quad [4]$$

Solution of eqn [4] yields

$$V = 2\pi w_0^2 Z' + \frac{2\lambda^2}{3\pi w_0^2} Z'^3 \quad [5]$$

The Gaussian volume expression contains two terms. The first term, $2\pi w_0^2 Z'$, corresponds to a central cylindrical volume; the second term has a more complex form that describes the extra curved volume (Figure 4b). The diffraction-limited beam waist radius w_0 can be defined in terms of the focusing objective focal length f , the refractive index n , and the collimated beam radius R according to

$$w_0 = \frac{\lambda f}{n\pi R} \quad [6]$$

Substitution in eqn [5] yields,

$$\begin{aligned} V &= 2\pi \left(\frac{\lambda f}{n\pi R} \right)^2 Z' + \frac{2\lambda^2}{3\pi} \left(\frac{n\pi R}{\lambda f} \right)^2 Z'^3 \\ &= \frac{2\lambda^2 f^2}{\pi n^2 R^2} Z' + \frac{2\pi n^2 R^2}{3f^2} Z'^3 \end{aligned} \quad [7]$$

The volume is now expressed in terms of identifiable experimental variables and constants. Once again, the first term may be correlated with the cylindrical contribution to the volume, and the second term is the

additional volume due to the curved contour. It is clear from Figure 4a that, for a given focal length, the noncylindrical contribution to the probe volume increases with incident beam diameter, when the diffraction limited focus is correspondingly sharp and narrow. Furthermore, it can also be seen that the second term in eqn [7] is inversely proportional to f^2 , and thus the extent to which the probe volume is underestimated by the cylindrical approximation increases with decreasing focal length. This fact is significant when performing confocal measurements, since high numerical aperture objectives with short focal lengths are typical. Some realistic experimental parameters give an indication of typical dimensions for the probe volume in confocal SMD systems. For example, if $\lambda = 488$ nm, $f = 1.6$ mm, $Z' = 1.0$ μ m and $n = 1.52$, a minimum optical probe volume of 1.1 fL is achievable with a collimated beam diameter of 1.1 mm.

Intensity Fluctuations: Photon Burst Statistics

When sampling a small volume within a system that may freely exchange particles with a large surrounding analyte bath, a Poisson distribution of particles is predicted. A Poisson distribution is a discrete series that is defined by a single parameter μ equating to the mean and variance of the distribution:

$$P(n = x) = \frac{\mu^x e^{-\mu}}{x!} \quad [8]$$

Common Poisson processes include radioactive disintegration, random walks and Brownian motion. Although particle number fluctuations in the excitation volume are Poissonian in nature, the corresponding fluorescence intensity modulation induces a stronger correlation between photon counts. For a single molecular species the model is described by two parameters: an intrinsic molecular brightness and the average occupancy of the observation volume. A super-Poissonian distribution has a width or variance that is greater than its mean; in a Poisson distribution the mean value and the variance are equal. The fractional deviation Q is defined as the scaled difference between the variance and the expectation value of the photon counts, and gives a measure of the broadening of the photon counting histogram (PCH). Q is directly proportional to the molecular brightness factor ε and the shape factor γ of the optical point spread function. (γ is constant for a given experimental geometry.)

$$Q = \frac{\langle \Delta n^2 \rangle - \langle n \rangle}{\langle n \rangle} = \gamma \varepsilon \quad [9]$$

A pure Poisson distribution has $Q = 0$; for super-Poissonian statistics $Q > 0$. Deviation from the Poisson function is maximized at low number density and high molecular brightness.

In a typical SMD experiment raw data are generally collected with a multichannel scalar and photons are registered in binned intervals. Figure 5

illustrates typical photon burst scans demonstrating the detection of single molecules (R-phycoerythrin) in solution. Fluorescence photon bursts, due to single molecule events, are clearly distinguished above a low background baseline (top panel) of less than 5 counts per channel in the raw data. It is noticeable that bursts vary in both height and size. This is in part due to the range of possible molecular trajectories through the probe volume, photobleaching kinetics, and the nonuniform illumination intensity in the probe region. In addition, it can be seen that the burst frequency decreases as bulk solution concentration is reduced. This effect is expected since the properties of any given single-molecule event are determined by molecular parameters alone (e.g., photophysical and diffusion constants) and concentration merely controls the frequency/number of events.

Although many fluorescence bursts are clearly distinguishable from the background, it is necessary to set a count threshold for peak discrimination in order to correctly identify fluorescence bursts above the background. A photocount distribution can be used as the starting point for determining an appropriate threshold for a given data set. The overlap between signal and background photocount distributions affects the efficiency of molecular detection. Figure 6 shows typical signal and background photocount probability distributions, with a threshold set at approximately 2 photocounts per channel. The probability of spurious (or false)

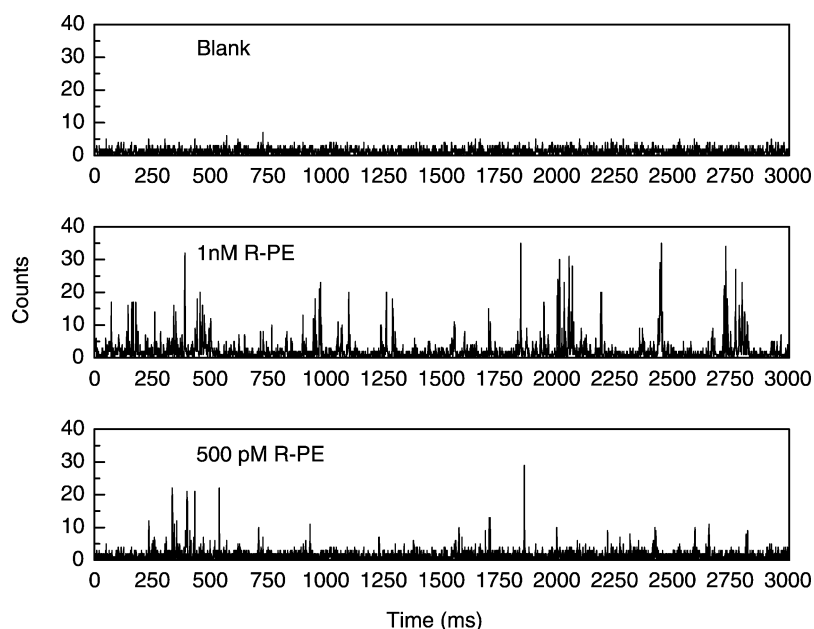


Figure 5 Photon burst scans originating from 1 nM and 500 pM R-phycoerythrin buffered solutions. Sample is contained within a 50 μm square fused silica capillary. Laser illumination = 5 μW , channel width = 1 ms. The top panel shows a similar burst scan originating from a deionized water sample measured under identical conditions.

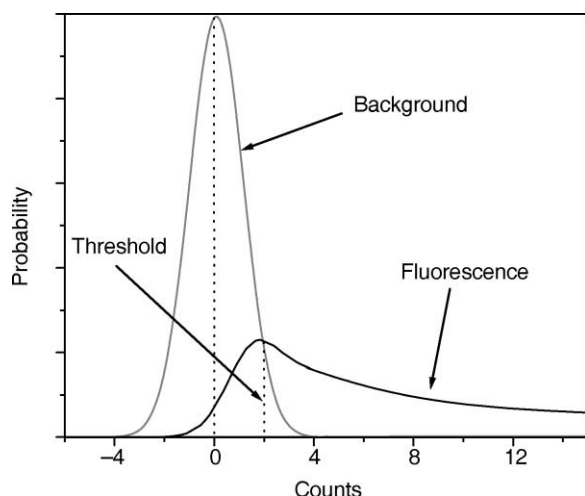


Figure 6 Simulated fluorescence and background photocount probability distributions. The vertical dashed line at 2 counts represents an arbitrarily defined threshold value for peak determination.

detection resulting from statistical fluctuations in the background can be quantified by the area under the 'background' curve at photocount values above the threshold. Similarly, the probability that 'true' single molecule events are neglected can be estimated by the area under the 'fluorescence' curve at photocount values below the threshold. Choice of a high threshold value will ensure a negligible probability of calling a false positive, but will also exclude a number of true single molecule events that lie below the threshold value. Conversely, a low threshold value will generate an unacceptably high number of false positives. Consequently, choice of an appropriate threshold is key in efficient SMD.

Since the background shot noise is expected to exhibit Poisson statistics, the early part of the photocount distribution (i.e., the portion that is dominated by low, background counts) can be modeled with a Poisson distribution, to set a statistical limit for the threshold. Photon counting events above this threshold can be defined as photon bursts associated with the presence of single molecules. In an analogy with Gaussian systems the selected peak discrimination threshold can be defined as three standard deviations from the mean count rate:

$$n_{\text{threshold}} = \mu + 3\sqrt{\mu} \quad [10]$$

Adoption of a threshold that lies 3 standard deviations above the mean yields a confidence limit that is typically greater than 99%. **Figure 7**

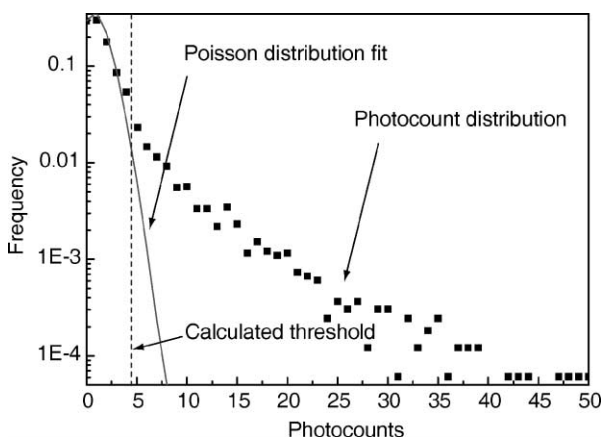


Figure 7 A photon counting histogram generated from a 16 second photon burst scan originating from a 10 $\mu\text{g/mL}$ solution of 1000 nm fluorescent microbeads. The dotted curve shows a least-squares fit of early channels to a Poisson distribution, and the dashed vertical line marks the peak threshold (defined as $\mu + 3\sqrt{\mu} = 4.47$ counts).

illustrates a sample photocount distribution, a least-squares fit to an appropriate Poisson distribution, and the calculated threshold that results. Once the threshold has been calculated, its value is subtracted from all channel counts and a peak search utility used to identify burst peaks in the resulting data set.

Data Filtering

As stated, the primary challenge in detecting single molecules in solution is not the maximization of the detected signal, but the maximization of the signal-to-noise ratio (or the reduction of background interferences). Improving the signal-to-noise ratio in such experiments is important, as background levels can often be extremely high.

Several approaches have been used to smooth SMD data with a view to improving signal-to-noise ratios. However, the efficacy of these methods is highly dependent on the quality of the raw data obtained in experiment. As examples, three common methods are briefly discussed. The first method involves the use of a weighted quadratic sum (WQS) smoothing filter. The WQS function creates a weighted sum of adjacent terms according to

$$\tilde{n}_{k,\text{WQS}} = \sum_{j=0}^{m-1} w_j (n_{k+j})^2 \quad [11]$$

The range of summation m is the same order as the burst width, and the weighting factors w_j are chosen

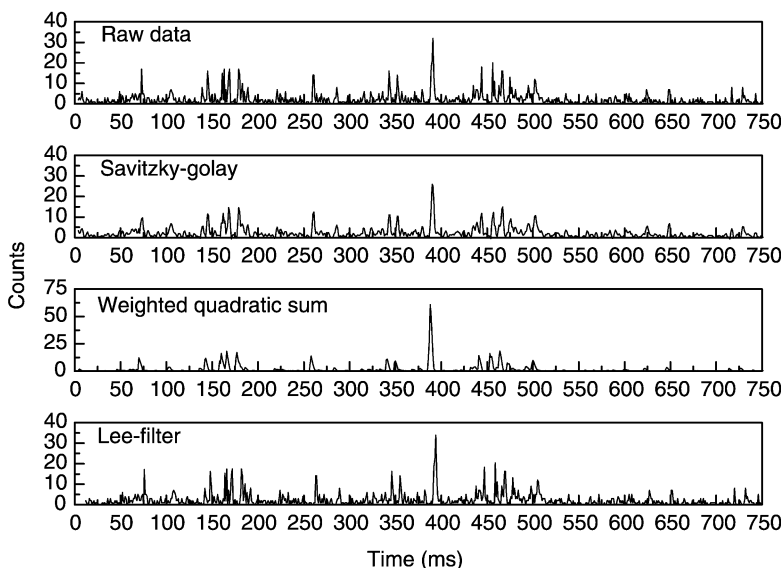


Figure 8 Effect of various smoothing filters on a 750 ms photon burst scan originating from a 1 nM R-phycoerythrin buffered solution. Raw data are shown in the top panel.

to best discriminate between single-molecule signals and random background fluctuations. This method proves most useful for noisy systems, in which the raw signal is weak. There is a practical drawback, in that peak positions are shifted by the smoothing function, and subsequent burst analysis is therefore hampered.

Another popular smoothing filter is the Lee-filtering algorithm. The Lee filter preferentially smooths background photon shot noise and is defined according to

$$\tilde{n}_k = \bar{n}_k + (n_k - \bar{n}_k) \frac{\sigma_k^2}{\sigma_k^2 + \sigma_0^2} \quad [12]$$

where the running mean (\bar{n}_k) and running variance (σ_k^2) are defined by

$$\bar{n}_k = \frac{1}{(2m+1)} \sum_{j=-m}^m n_{k+j} \quad m < k \leq N - m \quad [13]$$

$$\sigma_k^2 = \frac{1}{(2m+1)} \sum_{j=-m}^m (n_{k+j} - \bar{n}_{k+j})^2 \quad 2m < k \leq N - 2m \quad [14]$$

for a filter $(2m+1)$ channels wide. Here, n_k is the number of detected photons stored in a channel k , σ_0 is a constant filter parameter, and N is the total number of data points.

A final smoothing technique worth mentioning is the Savitzky-Golay smoothing filter. This filter uses a least-squares method to fit an underlying polynomial function (typically a quadratic or quartic function) within a moving window. This approach works well for smooth line profiles of a similar width to the filter window and tends to preserve features such as peak height, width and position, which may be lost by simple adjacent averaging techniques. Figure 8 shows the effects of using each approach to improve signal-to-noise for raw burst data.

Photon Burst Statistics

A valuable quantitative analysis method for analysis of fluorescence bursts utilizes the analysis of Poisson statistics. Burst interval distributions are predicted to follow a Poissonian model, in which peak separation frequencies adopt an exponential form. The probability of a single molecule (or particle) event occurring after an interval Δt is given by eqn [15]:

$$N(\Delta t) = \lambda \exp(-\beta t) \quad [15]$$

where λ is a proportionality constant and β is a characteristic frequency at which single molecule events occur. The recurrence time τ_R can then be simply defined as

$$\tau_R = \frac{1}{\beta} \quad [16]$$

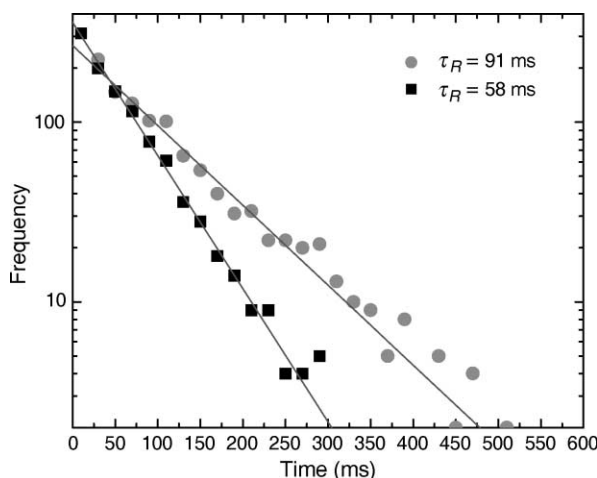


Figure 9 Burst interval distribution analysis of photon burst scans. Data originate from 1 μm fluorescent beads moving through 150 μm wide microchannels at flow rates of 200 nL min^{-1} (circles) and 1000 nL min^{-1} (squares). Least squares fits to a single exponential function are shown by the solid lines.

Equation [6] simply states that longer intervals between photon bursts are less probable than shorter intervals. Furthermore, the recurrence time reflects a combination of factors that control mobility, probe volume occupancy, or other parameters in the single molecule regime. Consequently, it is expected that τ_R should be inversely proportional to concentration, flow rate or solvent viscosity in a range of systems. **Figure 9** shows an example of frequency $N(\Delta t)$ versus time plots for two identical particle systems moving at different velocities through the probe volume. A least-squares fit to a single exponential function yields values of $\tau_R = 91$ ms for a volumetric flow rate of 200 nL/min and $\tau_R = 58$ ms for a volumetric flow rate of 1000 nL/min .

Temporal Fluctuations: Autocorrelation Analysis

Autocorrelation analysis is an extremely sensitive method for detecting the presence of fluorescence bursts in single molecule experiments. This approach essentially measures the average of a fluctuating signal as opposed to the mean spectral intensity. As previously discussed, the number of molecules contained within a probe volume at any given time is governed by Poisson statistics. Consequently, the root mean square fluctuation can be defined according to eqn [17],

$$\frac{\sqrt{\langle(\delta N)^2\rangle}}{\langle N \rangle} = \frac{\sqrt{\langle(N - \langle N \rangle)^2\rangle}}{\langle N \rangle} = \frac{1}{\sqrt{\langle N \rangle}} \quad [17]$$

where N is the number of molecules. It is observed that the relative fluctuation diminishes as the number of particles measured is increased. Hence, it is important to minimize the number of molecules present in the probe volume. It should be noted, however, that if there are too few molecules in the solution there will be long dark periods where no single molecule bursts are observed. If the probe volume is bathed in radiation of constant intensity, fluctuation of the resulting fluorescence signal can simply be defined as deviations from the temporal signal average:

$$\langle F(t) \rangle = \frac{1}{T} \int_0^T F(t) dt \quad [18]$$

Here, t is defined as the total measurement time, $F(t)$ is the fluorescence signal at time t , and $\langle F(t) \rangle$ is the temporal signal average. Fluctuations in the fluorescence intensity, $\delta F(t) = F(t) - \langle F(t) \rangle$, with time t , about an equilibrium value $\langle F \rangle$, can be statistically investigated by calculating the normalized autocorrelation function, $G(\tau)$, where

$$G(\tau) = \frac{\langle F(t + \tau)F(t) \rangle}{\langle F \rangle^2} = \frac{\langle \delta F(t + \tau)\delta F(t) \rangle}{\langle F \rangle^2} + 1 \quad [19]$$

In dedicated fluorescence correlation spectroscopy experiments, the autocorrelation curve is usually generated in real time in a high-speed digital correlator. Post data acquisition calculation is also possible using the following expression

$$G(\tau) = \sum_{t=0}^{N-1} g(t)g(t + \tau) \quad [20]$$

Here $g(t)$ is the total number of counts during the time interval $(t, t + \Delta t)$, $g(t + \tau)$ is the number of counts detected in an interval of Δt at a later time $t + \tau$, and N is the total number of time intervals in the dataset. In a diffusion controlled system with a single fluorescent molecule that is irradiated with a three dimensional Gaussian intensity profile, the autocorrelation curve is governed by the mean probe volume occupancy N and the characteristic diffusion time (τ_D). The laser beam waist radius ω and the probe depth $2z$ describe the Gaussian profile:

$$G(\tau) = 1 + \frac{1}{N} \left(1 + \frac{\tau}{\tau_d} \right)^{-1} \left(1 + \left(\frac{\omega}{z} \right)^2 \frac{\tau}{\tau_d} \right)^{-1/2} \quad [21]$$

The diffusion time is a characteristic molecular residence time in the probe volume and inversely

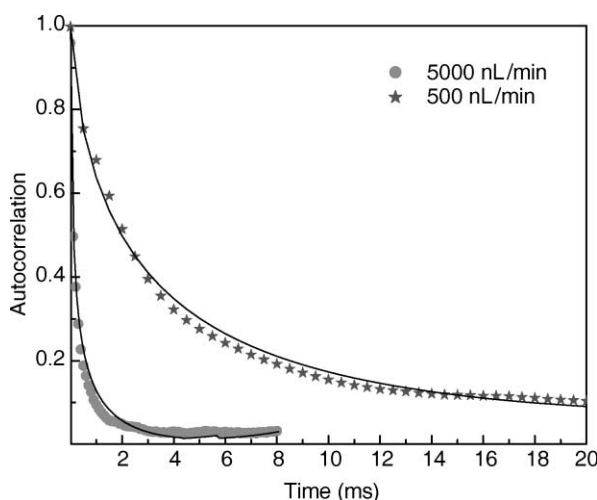


Figure 10 Autocorrelation analysis of photon burst scans of $1\text{ }\mu\text{m}$ fluorescent beads moving through $150\text{ }\mu\text{m}$ wide microchannels at flow rates of 500 nL min^{-1} (stars) and 1000 nL min^{-1} (circles). Solid lines represent fits to the data according to eqn [23].

related to the translational diffusion coefficient for the molecule:

$$D = \frac{w^2}{4\tau_D} \quad [22]$$

In a flowing system, the autocorrelation function depends on the average flow time through the probe volume τ_{flow} . A theoretical fit to the function can be described according to

$$G(\tau) = 1 + \frac{1}{N} A \exp\left\{\left(\frac{\tau}{\tau_{\text{flow}}}\right)^2 A\right\} \quad [23]$$

$$A = \left(1 + \frac{\tau}{\tau_d}\right)^{-1} \left(1 + \left(\frac{\omega}{z}\right)^2 \frac{\tau}{\tau_d}\right)$$

where N is the mean probe volume occupancy; the flow velocity v can then be extracted from the characteristic flow time according to

$$v = \frac{w}{\tau_{\text{flow}}} \quad [24]$$

It should be noted that in the case that directed flow is negligible or defined to be zero, the autocorrelation function simplifies to eqn [21].

Figure 10 illustrates experimentally determined autocorrelation curves for two identical particle systems moving at different velocities through the probe volume. As particle flow velocity is

increased, the width of the autocorrelation curves is seen to narrow as a result of the reduced residence time in the probe volume. A plot of the reciprocal of the full width half maximum of the autocorrelation curve as a function of volumetric flow rate is linear, and provides a simple way of calculating particle/molecule velocities within flowing systems.

Applications

The basic tools and methods outlined in this chapter have been used to perform SMD in a variety of chemically and biologically relevant systems, and indeed there is a large body of work describing the motion, conformational dynamics and interactions of individual molecules (see Further Reading). A primary application area has been in the field of DNA analysis, where SMD methods have been used in DNA fragment sizing, single-molecule DNA sequencing, high-throughput DNA screening, single-molecule immunoassays, and DNA sequence analysis. SMD methods have also proved highly useful in studying protein structure, protein folding, protein-molecule interactions, and enzyme activity.

More generally, SMD methods may prove to be highly important as a diagnostic tool in systems where an abundance of similar molecules masks the presence of distinct molecular anomalies that are markers in the early stages of disease or cancer.

See also

Microscopy: Confocal Microscopy.

Further Reading

- Ambrose WP, Goodwin PM, Jett JH, Van Orden A, Werner JH and Keller RA (1999) Single molecule fluorescence spectroscopy at ambient temperature. *Chem. Rev.* 99: 2929–2956.
- Barnes MD, Whitten WB and Ramsey JM (1995) Detecting single molecules in liquids. *Anal. Chem.* 67: 418A–423A.
- Basche T, Orrit M and Rigler R (2002) *Single Molecule Spectroscopy in Physics, Chemistry, and Biology*. New York: Springer-Verlag.
- Zander CJ, Enderlein J and Keller RA (2002) *Single Molecule Detection in Solution: Methods and Applications*. New York: John Wiley & Sons.